PAPER

A new approach for crystallization of copper(II) oxide hollow nanostructures with superior catalytic and magnetic response†

Inderjeet Singh,[a,b] Katharina Landfester,[b] Amreesh Chandra*[a] and Rafael Muñoz-Espí*[b,c]

We report the synthesis of copper(II) oxide hollow nanostructures at ambient pressure and close to room temperature by applying the soft templating effect provided by the confinement of droplets in miniemulsion systems. Particle growth can be explained by considering a mechanism that involves both diffusion and reaction control. The catalytic reduction of *p*-nitrophenol in aqueous media is used as a model reaction to prove the catalytic activity of the materials: the synthesized hollow structures show nearly 100 times higher rate constants than solid CuO microspheres. The kinetic behavior and the order of the reduction reaction change due to the increase of the surface area of the hollow structures. The synthesis also leads to modification of physical properties such as magnetism.

Introduction

The functionality of inorganic nanoparticles is strongly dependent on the degree of confinement (1-, 2- and 3-dimensional), which has a significant effect on the optical, electrical, mechanical, and thermal properties of the system.[1–6] It has also been reported that hierarchical assemblies and supramolecular structures can result in enhanced catalytic, energy storage, adsorption, and gas sensing capabilities.[7–13]

Controlled homogeneous, heterogeneous and cavitation-induced particle formation mechanisms in colloids are extensively explored for the synthesis of hierarchical nanostructures.[14–16] In all these mechanisms, the minimization of the Gibbs free energy is the driving force for the particle growth. Following the nucleation of the new phase, the growth is dependent on factors such as solute concentration, solvent, solubility, temperature, and pressure.[17,18] One of the strategies based on the homogeneous nucleation and cavitation mechanisms that is attaining prominence is the synthesis under droplet confinement in the presence of soft

[a]Department of Physics, Indian Institute of Technology, Kharagpur – 721302, West Bengal, India. E-mail: achandra@phy.iitkgp.ernet.in
[b]Max Planck Institute for Polymer Research, Ackermannweg 10, 55128 Mainz, Germany
[c]Institute of Materials Science (ICMUV), University of Valencia, PO Box 22085, 46071 Valencia, Spain. E-mail: rafael.munoz@uv.es
†Electronic supplementary information (ESI) available: Associated structural and morphological analysis, XPS characterization, BET surface area, catalytic measurements, recycle tests of the catalyst, and magnetic characterizations. See DOI: 10.1039/c5nr05579b

templates.[19–22] Under these conditions, the process is both reaction- and diffusion-controlled, which allows synthetic strategies for obtaining hollow inorganic nanostructures.[23,24] In such colloidal systems formed by nanodroplets, it is crucial to minimize aggregation, related to the system stability, and it is highly desirable to maintain the environment conditions as mild as possible. These requirements can be fulfilled by the use of the miniemulsion technique. In this process, kinetically stabilized emulsions of two immiscible liquids are homogenized by high-shear forces, typically in the presence of a surfactant. During the synthesis, particle formation takes place in nanodroplets that contain the precursors.[25–29]

Among transition metal oxides nanostructures, those based on copper(II) oxide find applications in very different areas, ranging from catalysis, antibacterial coatings or magnetic sensors to energy and semiconductor devices.[10,12,30–37] Synthesis routes being explored to prepare stable hierarchical, porous or hollow nanostructures of CuO have only led so far to the growth of micron-sized particles similar to those obtained in reactions under high temperature or pressure.[7,38,39] New strategies are thus required to achieve hollow CuO hierarchical nanostructures, which will have a significantly enhanced effective surface area when compared to solid nanoparticles, making them useful in applications such as catalysis.

In this paper, we present a successful strategy to synthesize hollow CuO nanostructures by taking the advantage of the crystallization at the interface of droplets in water-in-oil (w/o) miniemulsions under mild conditions. The growth mechanism, which is explained using a simple theoretically conceptualized model, is a convoluted picture of homogeneous growth

with contributions from reaction and diffusion controlled dynamics. A large increase in the catalytic activity is observed by the use of hollow nanostructures in comparison to corresponding solid microspheres. Finally, the work also shows that our materials have remarkably different magnetic response compared to microspheres.

Experimental section

Materials

Copper(II) nitrate trihydrate (Sigma-Aldrich, ≥99%), triethylamine (TEA, Sigma-Aldrich, ≥99.5%), p-nitrophenol (Sigma-Aldrich, ≥99%), sodium borohydride (Sigma-Aldrich, 99.99%), copper(II) oxide powder (12 nm) (Iolitec Nanomaterials, 99.5%), cupric oxide (Merck, >99%), polyglycerol polyricinoleate (PGPR, Danisco), and polyisobutylene succinimide pentamine (PIBSP, OS85737, Lubrizol France, Rouen) were used as received. Milli-Q water was used throughout the experiments.

Synthesis of CuO hollow nanostructures

A 1 wt% solution of the surfactant PIBSP in toluene was prepared and used as the continuous phase. The dispersed phase consisted of a 0.5 M solution of $Cu(NO_3)_2 \cdot 3H_2O$ in water. The dispersed and continuous phases were mixed in 1:4 weight ratio and pre-emulsified by stirring for 30 min at 1000 rpm. Afterward, the mixture was ultrasonified for 2 min (Branson Sonifier W-450D, $\frac{1}{2}''$ tip, 70% amplitude, 1 s pulse, 0.1 s pause) while cooling in an ice-water bath. TEA (3 equivalents with respect to the Cu(II) precursor) was rapidly added by using a syringe. The emulsion was kept under stirring for 4 h at 1000 rpm at 80 °C to ensure homogenization and completion of the precipitation reaction. The powders were separated from the dispersion by centrifugation for 20 min at 4000 rpm. To remove unreacted reagents and reaction byproducts, the obtained powders were washed by centrifugation (10 min, 4000 rpm) with ethanol (twice), deionized water (twice) and acetone (once). For investigating the properties such as catalysis and magnetism, dense CuO was obtained by thermal treatment of the powders at 250 °C.

Reduction catalysis experiments

30 μL of a p-nitrophenol aqueous solution (10^{-2} M), 200 μL of freshly prepared aqueous NaBH$_4$ solution (10^{-4} M), and 2.77 mL of water were placed in a quartz cuvette and homogenized. The final concentrations of p-nitrophenol and NaBH$_4$ were 10^{-4} M and 6.7×10^{-3} M, respectively. The CuO powders were added to this solution in concentration of 1, 2, or 4 mg mL^{-1}. UV-Vis spectra of the solutions were recorded at fixed time intervals in the 200 nm–500 nm range (Perkin-Elmer UV-Vis spectrophotometer), instantly after the addition of CuO powders. The degradation of the p-nitrophenolate ions was investigated by monitoring the changes in the UV-Vis absorption spectra.

Reusability of the catalytic nanostructures was investigated for up to 4 cycles of operation. For the recycling process, nano-

particles used in the previous cycle were collected by high speed centrifugation and washed 3 times with deionized water to remove the adsorbed acetophenolate ions. Prior to experiments, the washed powders were dried in vacuum oven at 70 °C for 12 h.

Characterization methods

The powder X-ray diffraction patterns were collected using a PANalytical high resolution diffractometer PW 3040/60 with Cu Kα radiation (λ = 1.54 Å) as incident wavelength. The diffraction pattern was collected in the 2θ range 10–100° and the structure refinement was performed using the Fullprof refinement software.[40,41]

Scanning electron microscope (SEM) images were obtained using a field-emission microscope Leo Gemini model 1530 and the transmission electron microscopy (TEM) was carried out using a JEOL 1400 microscope. A small amount of the colloidal dispersion was diluted in an identical organic phase and drop-casted onto a silicon wafer for SEM and onto a carbon coated Cu grids for TEM measurements.

Magnetic measurements were performed using a Quantum Design Ever Cool SQUID VSM DC magnetometer. Hysteresis curves were recorded at 5, 50, 150, 250, and 300 K with magnetic fields up to 6 T. Zero field cooled (ZFC) and field cooled (FC) curves were measured from 380 to 5 K temperature at an applied field of 100 Oe.

Results and discussion

Crystal structure, morphology, and growth mechanism

The hollow nanostructures studied here were synthesized by precipitation of a copper(II) salt in confined droplets of an inverse miniemulsion system. The particle formation takes place at the interface between water and oil in the dispersed droplets. Fig. 1(a) shows the X-ray diffraction pattern of powders obtained from miniemulsions prepared with the surfactant PIBSP after addition of triethylamine (TEA). Although the tenorite CuO phase can be stabilized even at room temperature and ambient pressure (see the CuO peaks marked in Fig. 1(a), JCPDS Card no. 04-009-2287), coexistence of $Cu(OH)_2$ was also observed in the samples. In contrast, when the precipitation reaction was carried out at 80 °C, CuO was the only obtained phase, as shown in Fig. 1(b). XRD patterns could be refined using the monoclinic space group $C2/c$.[42] The quality of the structure refinement can be seen from the nearly flat difference profile.

For removal of the surfactant and to induce densification, a certain quantity of the prepared powders was also treated at 250 °C. The XRD pattern for the sample (Fig. S1†) is similar to that of the as prepared powders (Fig. 1(b)) but with a slight peak sharpening. Typical crystallite sizes calculated using the Scherrer equation for powders obtained at 80 °C in emulsion and densified at 250 °C were 23 and 28 nm, respectively. The oxidation state +2 of copper in the powders was confirmed
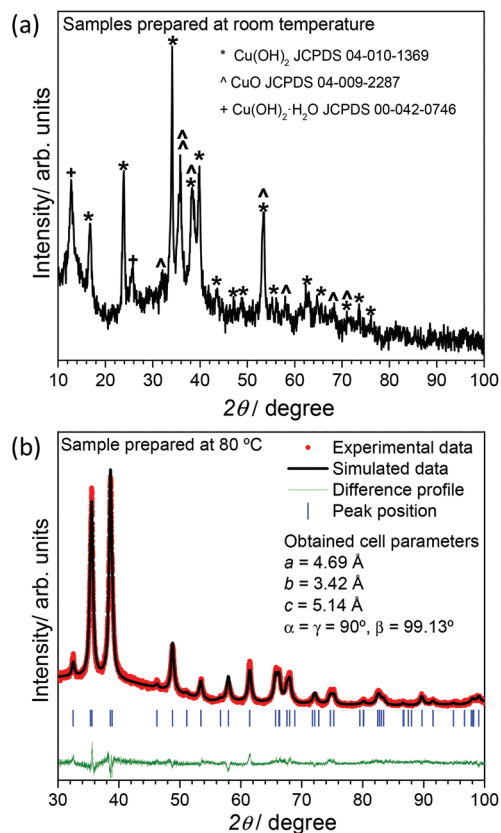
Fig. 1 (a) XRD pattern of as-obtained precipitated powders, (b) XRD pattern of the powders obtained after heating the emulsion at 80 °C, (b) the blue bars depict the expected peak positions, red coloured circles and the solid black line represent the observed and simulated data profiles. The green solid line shows the difference profile.

Fig. 2 TEM image of the as-prepared hollow CuO nanostructures.

from the peak positions and profile fitting of core level Cu2p XPS spectra (see details in Fig. S2†).

A TEM micrograph for the CuO particles precipitated at 80 °C is shown in Fig. 2 (see also micrographs of samples precipitated at room temperature in Fig. S3†). Consistent with an interfacial precipitation mechanism, the micrograph shows the formation of hollow structures. The structure is formed by the entanglement of needles or rods (∼10 nm diameter), residing at the perimeter of the interface.

In most colloidal systems, following the nucleation, the particle growth starts, leading to the formation of a solid grain that is an agglomeration of smaller particles. This is clearly not the case in the present growth mechanism, in which the particles formed at the interface of nanodroplets with restricted growth. The mechanism of particle formation is analogous to the reported by Bourret and Lennox,[38] who have suggested mesoscale aggregation at the interface for obtaining micron-sized hollow structures of CuO. However, in our case, the final structures are smaller by two orders of magnitude because of the confined droplet size in the miniemulsion system.

The proposed growth mechanism is schematically shown in Fig. 3. In the initial phase, the amine groups of the PIBSP sur-
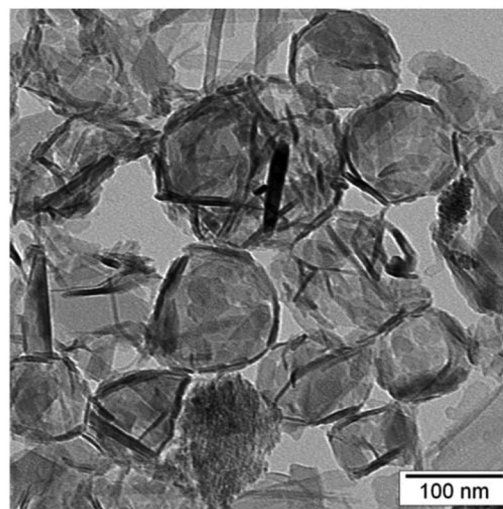
factant available at the interface act as chelating agents, interacting with the metallic Cu^{2+} ions and leading to the increase of their concentration at the interface. This complexation of Cu^{2+} ions by the amine groups of the surfactant stimulate nucleation sites at the liquid–liquid interface for the initiation of the particle growth. As mentioned earlier, the reaction is initiated by the prompt addition of the partially water-soluble base TEA. The rapid increase in the concentration of OH^- ions at the interface promotes the precipitation process at the phase boundary. Initially, very small sized particles are expected to grow uniformly, but the presence of the surfactant along with the metallic complexes results in an anisotropic growth of the precipitated CuO particles. Therefore, following constant stirring, these small sized particles will anisotropically coagulate to give solid rod-like nanostructures interconnected with each other at the droplet interface. While the reaction is mainly happening at the interface, certain fraction of TEA is expected to diffuse in the water trapped within the droplet, which could result in the formation of few particles inside the central hollow area.

The importance of the amino groups present in the surfactant for the formation of the hollow morphologies was verified by comparing the results of analogous experiments with the surfactant polyglycerol polyricinoleate (PGPR), which does not have amine groups. In the case of PGPR, the crystallized CuO nanostructures do not show a hollow morphology, which is explained by the non-occurrence of the complexation of Cu(II) ions by the surfactant at the droplet interface (see details in ESI, Fig. S4†).

Catalysis of the degradation of *p*-nitrophenol

p-Nitrophenol is a pollutant extensively present in the industrial waste-water streams. Use of catalytic nanoparticles for initiating the reduction process of the *p*-nitrophenol is extensively explored. The catalytic activity of hollow CuO
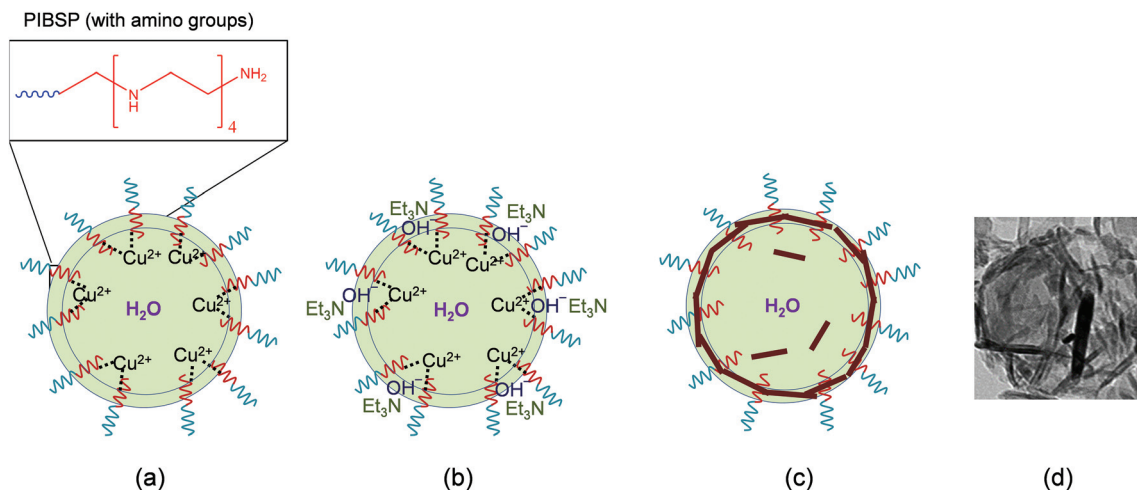
Fig. 3 Scheme of the formation mechanism of CuO nanostructures using PIBSP as surfactant: (a) representation of droplet with surfactant and precursor ions, (b) precipitation at the interface upon addition of TEA, (c) growth of particles at the interface, and (d) actual TEM image.

nanostructures was investigated for the degradation of p-nitrophenol to p-aminophenol in the presence of $NaBH_4$. As references, we also used commercial solid CuO nanoparticles of 12 nm and CuO microspheres. The surface area is known to have significant effect on the catalytic properties. Therefore, the specific surface areas and porosity for our samples and the commercial references were calculated by the analysis of adsorption–desorption BET isotherms, shown in Fig. 4(a, b). The isotherms were recorded for as-prepared samples and for samples calcined at 250 °C. Isotherms in Fig. 4(a) suggest the presence of macropores in both as-prepared and calcined samples (see the corresponding pore size distribution shown in Fig. 4(b)). The values of specific surface area for as-prepared and calcined hollow nanostructures were found to be ∼20 $m^2 g^{-1}$ and ∼85 $m^2 g^{-1}$, respectively, which are significantly higher than conventional commercial solid CuO nanoparticles of 12 nm (∼48 $m^2 g^{-1}$) and CuO microspheres (∼4 $m^2 g^{-1}$) (see details in Fig. S5†). As the specific surface area increases ∼4 times upon removal of the surfactant, calcined powders were used for the catalytic experiments.

UV-Vis spectra of light yellow p-nitrophenol solution show an absorption peak centered at 317 nm (see ESI, Fig. S6(a)†). The addition of $NaBH_4$ initiates the formation of p-nitrophenolate ions and the absorption peak at 317 nm shifts to ∼400 nm. The formation of p-nitrophenolate ions transforms the color of the solution from light to dark yellow. After the conversion to p-nitrophenolate ions, no further reduction was observed with time (see ESI, Fig. S6(b)†).[43] In the presence of hollow CuO nanostructures (1 mg mL^{-1}), the transformation of p-nitrophenolate to p-aminophenol was monitored by the decrease of the absorption peak at 400 nm and the appearance of a new peak at ∼300 nm, as shown in Fig. 5(a) (see UV-Vis spectra for the commercial CuO references in Fig. S6(c–e)†). Macroscopically, the degradation of p-nitrophenol can be observed from the color change from yellow to colorless. Once
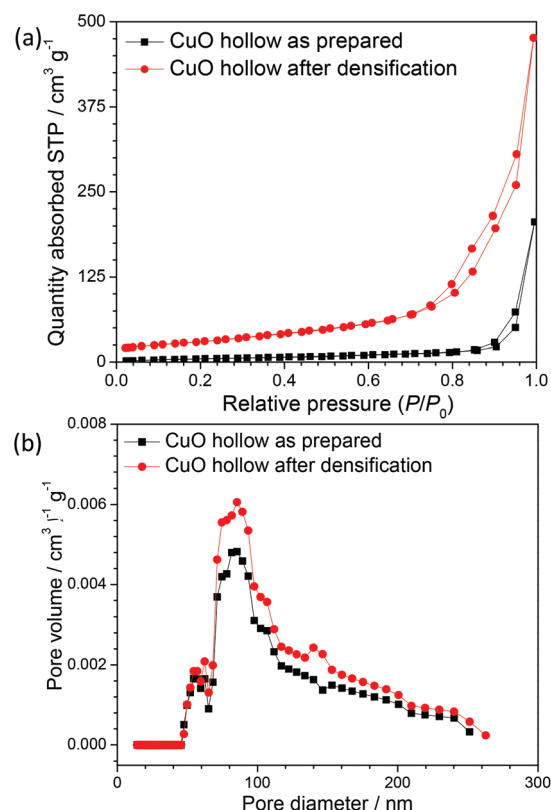

Fig. 4 (a) Adsorption–desorption isotherms and (b) pore size distribution curves for hollow CuO nanostructures.

the reduction reaction is completed, the absorption peak at 400 nm disappears completely.

Interestingly, a concentration of 2 mg mL^{-1} (double than the used for our hollow nanostructures) of commercial CuO microspheres could not reduce p-nitrophenol completely, even
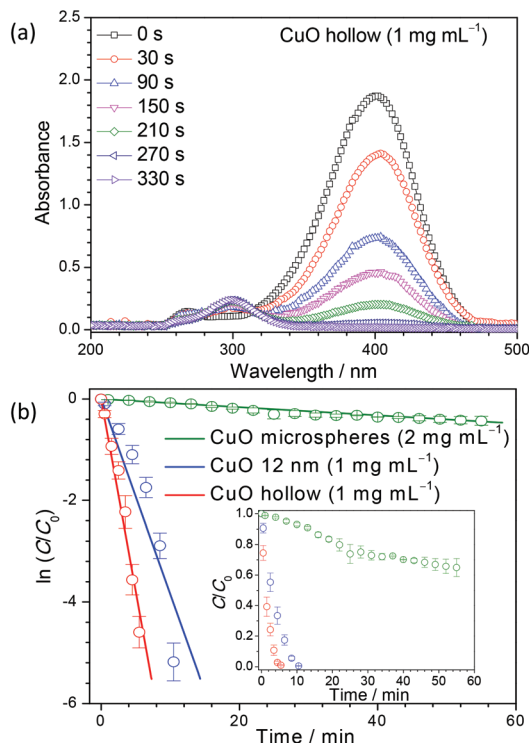
Fig. 5 UV-Vis spectra for *p*-nitrophenol reduction with (a) CuO hollow nanostructures, (b) $\ln(C/C_0)$ *versus* time curves for rate constants using different CuO catalysts. The inset shows the variation of C/C_0 *versus* time (error bars represent standard deviations from three measurements).

Table 1 Rate constants for reduction of *p*-nitrophenol using commercial and synthesized CuO nanostructures

Catalyst	Cycle	Catalyst concentration (mg mL^{-1})	Rate constant (s^{-1})
Commercial CuO microspheres	1	2	1.3×10^{-4}
Commercial 12 nm CuO particles	1	1	6.4×10^{-3}
CuO hollow nanostructures	1	1	1.3×10^{-2}
CuO hollow nanostructures	2	1	8.6×10^{-3}
CuO hollow nanostructures	3	1	8.3×10^{-3}
CuO hollow nanostructures	4	1	8.2×10^{-3}

Fig. 6 Scheme showing the catalytic process of *p*-nitrophenol reduction on the CuO surface.

after 1 h. A higher concentration of 4 mg mL^{-1} is required for the complete reduction, which occurs after 28 min (see details in Fig. S6(c, d)†). For 12 nm commercial CuO nanoparticles at a concentration of 1 mg mL^{-1}, the completion of the reduction process took more than 10 min (Fig. S6(e)†). In comparison, a concentration of only 1 mg mL^{-1} of the synthesized hollow CuO powders can completely reduce *p*-nitrophenol in about 5 min (Fig. 5(a)). These results demonstrate that the performance of our hollow CuO is much higher than the 12 nm commercially available nanoparticles. This large increase in the catalytic activity is directly associated with a large increase in the surface area. The concentration of NaBH$_4$ was kept high as compared to that of *p*-nitrophenolate ions, so that the reaction rate is nearly independent of the NaBH$_4$ concentration, and the reaction is assumed to follow a pseudo-first order kinetics.[44] The reaction rate can be calculated from the variation of the ratio of the concentration of *p*-nitrophenolate ions at a given time (C) to the initial concentration (C_0) with time (t). The variation of $\ln(C/C_0)$ *versus* time for the different catalysts is shown in Fig. 5(b). The slope of the curve gives directly the rate constant for the reaction, which are listed in Table 1. The results suggest an increase of nearly 100 times in the reaction rate constant when the hollow CuO nanoparticles are employed as compared to commercially available CuO microspheres. This very high rate constant is comparable to those

obtained with other reported expensive metal or metal oxide composites in heterogeneous catalysis (Table S1†). This finding can have significant implications for the industrial application of CuO based nanostructures in catalysis.

The suggested mechanism of the above discussed catalysis procedure is schematically shown in Fig. 6. *p*-Nitrophenol ions attain an equilibrium state following the adsorption and desorption from the active sites on the CuO surface. Once adsorbed on to the surface, *p*-nitrophenol reacts and is reduced to *p*-aminophenol, which can desorb in solution.

In catalysts with a very high number of active sites, which is typical for metallic catalysts, the rates of adsorption and desorption of *p*-nitrophenol are comparable.[45] Accordingly, adsorption of the reactant to the CuO surface depends largely on the reactant concentration and the reaction is considered to follow a pseudo-first order kinetics. Kong *et al.*[45] reported that, in case of a metal-free nitrogen-doped graphene catalyst, in which the number of active sites is much lower than for a metallic catalyst, the reaction follows a pseudo-zero order kinetics. In the work of Kong *et al.*, due to lower number of active sites on the catalyst, the rate of adsorption of *p*-nitrophenol is much higher than the desorption. Therefore, the rate of adsorption of *p*-nitrophenol on catalyst depends on the available active sites on the catalyst instead of their concentration.

To understand the observed increase in the catalytic activity of the CuO hollow nanostructures in comparison to the used references, we compared the kinetic behavior for complete degradation of *p*-nitrophenol, shown in Fig. 7. For the
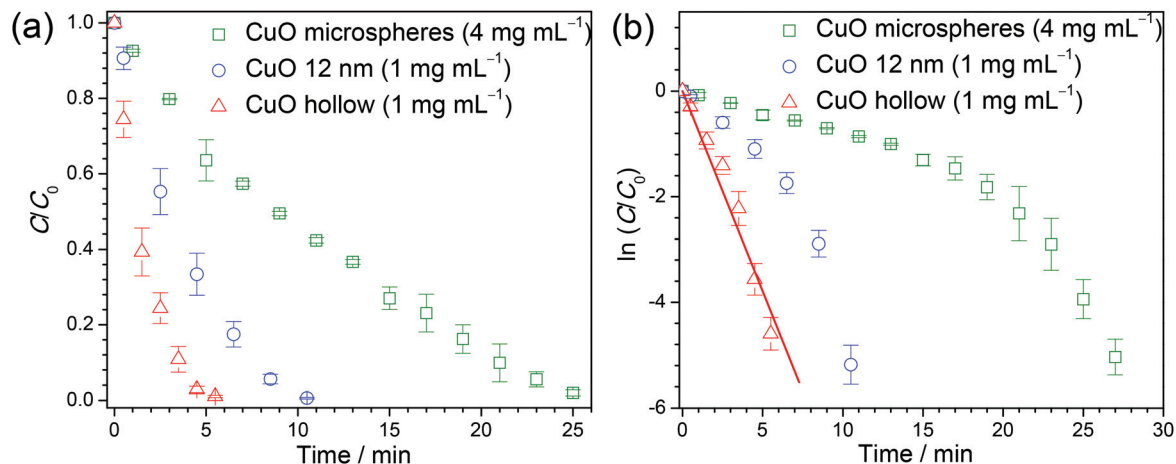
Fig. 7 Comparison of the variation of (a) C/C_0 (b) $\ln(C/C_0)$ with time using different CuO catalysts for complete degradation of p-nitrophenol (error bars represent standard deviations from three measurements).

commercial CuO microspheres, to achieve a complete degradation a concentration of 4 mg mL^{-1} (a factor of 4 higher than for the other samples) is required. The change of the ratio of the product concentration (C/C_0) with time approaches to a linear behavior for the commercial microspheres, which would be consistent with a pseudo-zero order kinetics.[45] In contrast, for our hollow nanostructures, a linear trend is achieved for the variation of $\ln(C/C_0)$ $vs.$ time, but not for C/C_0 $vs.$ time, which would correspond to a pseudo-first order reaction. The kinetic behavior of the 12 nm particles is intermediate between the commercial microspheres and our hollow nanostructures.

For industrial application, the reusability of catalytic particles is important. CuO hollow powders could induce nearly 100% reduction for up to four cycles of measurements (see details in Fig. S7†). The rate of reaction decreased slightly for the second cycle and remained almost stable thereafter (from 1.3×10^{-2} to $ca.$ 8.6×10^{-3} s^{-1}, see Table 1). This decrease can be attributed to a decrease in the number of active sites on CuO after the first cycle due to a possible adsorption of p-aminophenol on some active sites. To further understand this behavior, XRD patterns of the catalyst were collected after the 4 catalytic cycles (see Fig. S8†). Previous reports on the usage of copper-based oxides for reduction of p-nitrophenol suggest a significant conversion of CuO and Cu$_2$O powders in metallic Cu following the reactions.[46,47] This is attributed to the presence of the strong reducing agent NaBH$_4$ in the reaction medium, which reduces Cu^{2+} and Cu$^+$ into metallic Cu. XRD patterns reaffirms that CuO materials continue to maintain crystalline nature after the different cycles, but there is a signature of a small peak arising at 43.3° from the metallic Cu. The appearance of Cu^0 in copper oxide-based catalysts has been sometimes related with an increase of the catalytic activity.[46] However, other works have shown that, as in our case, there is a decrease after the Cu^0 formation.[47]

Magnetism

The modifications in the surface and density of states will directly modify the physical properties of a particle. CuO is now being considered as a multiferroic material with significant application in spintronics, storage, sensing, etc.[48–51] Room temperature ferromagnetism (FM) and superparamagnetic blocking behavior have been observed in nanometric CuO.[33,52–55] The magnetic response of the hollow CuO nanoparticles was found to show ferromagnetic to antiferromagnetic transition in the low temperature regime (Fig. 8). This behavior is different from that reported for other types of CuO nanostructures, in which an anomalous response is observed. The authors of these works have tried to explain the behavior using the concepts of defects and blocking temperatures.[6,33]

It is now well understood that, as the size of the magnetic nanoparticles decreases up to sizes comparable to the order of magnitude of the domain wall width or the exchange length, large energy is required for the formation of domain walls. Therefore, the magnetic system prefers to remain in the so-called single domain state (also termed as elongated grains or mesocrystals) and show a hysteresis loop that is quite different from that observed in corresponding bulk systems.[27,56–59] The temperature-dependent variation of the magnetic parameters in hollow CuO nanostructures is given in Fig. 8 (b and c). From these curves, it could be inferred that CuO powders show ferromagnetic (FM) behavior at room temperature along with a paramagnetic (PM) contribution. Subtraction of this PM contribution from the whole data gives the FM character of the CuO nanostructures. The PM contribution can be estimated by linearly fitting the data observed at higher magnetic fields. M–H curves after the removal of the PM contribution are shown in Fig. 8(c). From these curves, a coercive field of 273 Oe with remanant magnetization of 0.023 emu g^{-1} could be
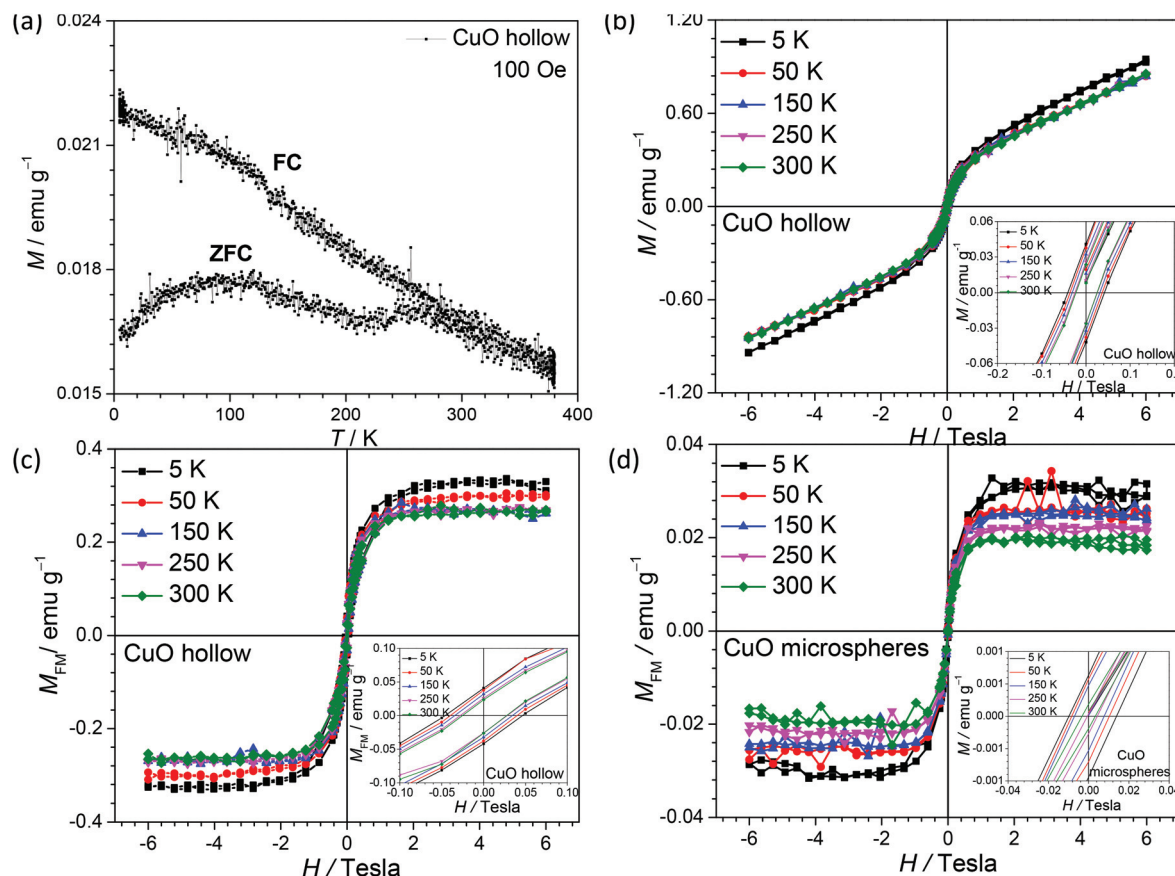
Fig. 8 Magnetic measurements of hollow CuO nanostructures (a) ZFC-FC curves measured from 5–380 K with field of 100 Oe, (b) M–H curves at 5, 50, 150, 250, and 300 K in field up to 6 T (c) M–H curves of CuO powders after subtracting paramagnetic contribution (d) M–H curves for CuO microspheres after substracting paramagnetic correction.

estimated. Saturation magnetization value of 0.27 emu g^{-1} was observed at room temperature, which is much higher (~10 times) than the found for commercial CuO microspheres (Fig. 8(d)) and previously reported values for CuO nano-structures (see magnetization curves for CuO microspheres in Fig. S9†).[33,53] This can be directly explained using the Stoner–Wohlfarth theoretical model, which predicts reduction in energy required for the alignment of the elongated grains.[56] The values for coercive field, remnant and saturation magnetization increase at lower temperatures as can be seen from the M–H curves.

Fig. 8(a) shows that the ZFC-FC curves coincide at high temperatures before they start diverging below 250 K. Similar to earlier reports, a ferromagnetic (FM) to anitiferromagnetic (AFM) transition is observed near 230 K.[60,61] A slight change in the slope of ZFC curve is observed near 225 K, which is directly associated with the spin realignment near the FM-AFM transition. CuO nanoparticles with size of ~5 nm and ~3 nm, in which finite size effects are more dominant, have been reported to show Neel temperatures of 30 and 13 K, respectively.[62] However, in our case, nanorods assemble to give a structure of 50–100 nm, and these effects are significantly suppressed. Furthermore, the ZFC curve below 230 K show a

decreasing trend, as expected for an AFM transition. In many other reports on magnetic response of CuO nanostructures, this behavior is not observed and the ZFC curve continues to show a rising trend.[53,55] The authors of these reports have attributed such anomalous behavior in terms of defect induced behavior.[53,55] In our system, as the particle size is quite uniformly distributed and the system has been obtained under milder conditions, the effect of defects will be less prominent, which allows the system to return a conventional ZFC-FC behavior.

Occurrence of both FM and superparamagnetism in CuO nanoparticles has been attributed to the presence of oxygen vacancies and uncompensated spins at the surface.[33,53,55] As seen in the XPS spectra analysis of synthesized hollow CuO powders (Fig. S2†), Cu(I) oxidation state was absent on the sample surface and no contribution other than that from O^{2-} and adsorbed oxygen was observed in the O 1s spectra. This excludes any possibility of vacancy-mediated magnetism in the synthesized samples. Therefore, the observed room temperature ferromagnetism can be linked to the presence of uncompensated surface spins. In AFM nanoparticles, the increase in uncompensated spins on the surface can induce a net magnetic moment.[6] Neel proposed that any imbalance of

'up' and 'down' spins at the surface would lead to a net magnetic moment in the antiferromagnetic materials.[63] In the present study, a much higher value of net magnetic moment in CuO was observed as compared to previous studies,[33,53,55] which can be related to higher number of uncompensated spins at the nanoparticles surface because of a low degree of agglomeration and higher available surface.

Conclusions

It has been unambiguously shown that crystallization of CuO can be achieved at the liquid–liquid interface of droplets in inverse miniemulsions to form hollow nanostructures. A homogeneous nucleation growth mechanism can be explained as a convoluted picture of reaction and diffusion controlled processes. The synthesized CuO hollow nanostructures have much higher surface areas than commercially available solid powders. The surface area enhancement results in a large increase of the catalytic activity, as proven for the catalytic reduction of p-nitrophenol. The large increment in reaction rate constants is related with a change in the reaction order kinetics upon surface area enhancement. Additionally, CuO show a large value of the ferromagnetic response at room temperature, which would make the material suitable for application in magnetic devices. The strategy of using inverse miniemulsion for the synthesis of crystalline hollow nanostructures under mild conditions opens up a new area for further improvements in the field of preparation of hollow functional materials.

Acknowledgements

References

1 A. D. Yoffe, *Adv. Phys.*, 2002, **51**, 799–890.
2 H. Yu, J. Li, R. A. Loomis, L. W. Wang and W. E. Buhro, *Nat. Mater.*, 2003, **2**, 517–520.
3 N. Satoh, T. Nakashima, K. Kamikura and K. Yamamoto, *Nat. Nanotechnol.*, 2008, **3**, 106–111.
4 D. Guo, G. Xie and J. Luo, *J. Phys. D: Appl. Phys.*, 2014, **47**, 013001.
5 H. E. Patel, S. K. Das, T. Sundararajan, A. S. Nair, B. George and a. T. Pradeep, *Appl. Phys. Lett.*, 2003, **83**, 2931.
6 D. P. Dutta, G. Sharma, P. K. Manna, A. K. Tyagi and S. M. Yusuf, *Nanotechnology*, 2008, **19**, 245609.
7 Z. Zhang, H. Che, Y. Wang, L. Song, Z. Zhongb and F. Su, *Catal. Sci. Technol.*, 2012, **2**, 1953–1960.
8 Y. Zhao, X. Song, Z. Yin and Q. Song, *J. Colloid Interface Sci.*, 2013, **396**, 29–38.
9 G. Qiu, S. Dharmarathna, Y. Zhang, N. Opembe, H. Huang and S. L. Suib, *J. Phys. Chem. C*, 2012, **116**, 468–477.
10 S.-F. Zheng, J.-S. Hu, L.-S. Zhong, W.-G. Song, L.-J. Wan and a. Y.-G. Guo, *Chem. Mater.*, 2008, **20**, 3617–3622.
11 Z. Yuan, Y. Wang and Y. Qian, *R. Soc. Chem. Adv.*, 2012, **2**, 8602–8605.
12 B. Wang, X.-L. Wu, C.-Y. Shu, Y.-G. Guo and C.-R. Wang, *J. Mater. Chem.*, 2010, **20**, 10661.
13 Y. Qin, F. Zhang, Y. Chen, Y. Zhou, J. Li, A. Zhu, Y. Luo, Y. Tian and J. Yang, *J. Phys. Chem. C*, 2012, **116**, 11994–12000.
14 L. Carbone and P. D. Cozzoli, *Nano Today*, 2010, **5**, 449–493.
15 Z. R. Tian, J. A. Voigt, J. Liu, B. McKenzie, M. J. McDermott, M. A. Rodriguez, H. Konishi and H. Xu, *Nat. Mater.*, 2003, **2**, 821–826.
16 S. Manickam and M. Ashokkumar, *Cavitation: A Novel Energy-Efficient Technique for the Generation of Nanomaterials*, CRC Press, 2014.
17 J. Charles P. Poole and F. J. Owens, *Introduction to Nanotechnology*, John Wiley & Sons, 2003.
18 S. K. Kulkarni, *Nanotechnology: Principles and Practices*, Springer, 2015.
19 M. Sivakumar, A. Towata, K. Yasui, T. Tuziuti and Y. Iida, *Curr. Appl. Phys.*, 2006, **6**, 591–593.
20 B. R. Reddy, T. Sivasankar, M. Sivakumar and V. S. Moholkar, *Ultrason. Sonochem.*, 2010, **17**, 416–426.
21 J. Eastoe, M. J. Hollamby and L. Hudson, *Adv. Colloid Interface Sci.*, 2006, **128–130**, 5–15.
22 R. Muñoz-Espí, Y. Mastai, S. Gross and K. Landfester, *CrystEngComm*, 2013, **15**, 2175.
23 F. Caruso, *Colloids and Colloid Assemblies: Synthesis, Modification, Organization and Utilization of Colloid Particles*, Wiley-VCH, 2004.
24 F. Caruso, *Modern Techniques for Nano- and Microreactors/reactions*, Springer, 2010.
25 R. Muñoz-Espí, C. K. Weiss and K. Landfester, *Curr. Opin. Colloid Interface Sci.*, 2012, **17**, 212–224.
26 M. Hajir, P. Dolcet, V. Fischer, J. Holzinger, K. Landfester and R. Muñoz-Espí, *J. Mater. Chem.*, 2012, **22**, 5622–5628.
27 I. Singh, A. K. Nigam, K. Landfester, R. Muñoz-Espí and A. Chandra, *Appl. Phys. Lett.*, 2013, **103**, 182902.
28 P. Dolcet, F. Latini, M. Casarin, A. Speghini, E. Tondello, C. Foss, S. Diodati, L. Verin, A. Motta and S. Gross, *Eur. J. Inorg. Chem.*, 2013, **2013**, 2291–2300.

29 P. Dolcet, C. Maurizio, M. Casarin, L. Pandolfo, S. Gialanella, D. Badocco, P. Pastore, A. Speghini and S. Gross, *Eur. J. Inorg. Chem.*, 2015, **2015**, 706–714.

30 Y. Feng and X. Zheng, *Nano Lett.*, 2010, **10**, 4762–4766.

31 F. M. Auxilia, S. Ishihara, S. Mandal, T. Tanabe, G. Saravanan, G. V. Ramesh, N. Umezawa, T. Hara, Y. Xu, S. Hishita, Y. Yamauchi, A. Dakshanamoorthy, J. P. Hill, K. Ariga and H. Abe, *Adv. Mater.*, 2014, **26**, 4481–4485.

32 X. Zhang, W. Shi, J. Zhu, D. J. Kharistal, W. Zhao, B. S. Lalia, H. H. Hng and a. Q. Yan, *ACS Nano*, 2011, **5**, 2013–2019.

33 G. N. Rao, Y. D. Yao and J. W. Chen, *J. Appl. Phys.*, 2009, **105**, 093901.

34 Y. Xia, X. Pu, J. Liu, J. Liang, P. Liu, X. Li and X. Yu, *J. Mater. Chem. A*, 2014, **2**, 6796.

35 S. Masudy-Panah, G. K. Dalapati, K. Radhakrishnan, A. Kumar, H. R. Tan, E. Naveen Kumar, C. Vijila, C. C. Tan and D. Chi, *Prog. Photovolt.: Res. Appl.*, 2015, **23**, 637–645.

36 G. Applerot, J. Lellouche, A. Lipovsky, Y. Nitzan, R. Lubart, A. Gedanken and E. Banin, *Small*, 2012, **8**, 3326–3337.

37 W. Wang, J. Wang, Z. Wang, X. Wei, L. Liu, Q. Ren, W. Gao, Y. Liang and H. Shi, *Dalton Trans.*, 2014, **43**, 6735–6743.

38 G. R. Bourret and R. B. Lennox, *J. Am. Chem. Soc.*, 2010, **132**, 6657–6659.

39 B. Liu and H. C. Zeng, *J. Am. Chem. Soc.*, 2004, **126**, 8124–8125.

40 J. R. Carvajal, Abstracts of the Satellite Meeting on Powder Diffraction of the XV Congress of the IUCr, 1990.

41 J. Rodriguez-Carvajal, *Physica B*, 1993, **192**, 55.

42 S. Asbrink and L.-J. Norrby, *Acta Crystallogr., Sect. B: Struct. Sci.*, 1970, **26**, 8–15.

43 K. Hayakawa, T. Yoshimura and K. Esumi, *Langmuir*, 2003, **19**, 5517.

44 R. W. J. Scott, O. M. Wilson and R. M. Crooks, *J. Phys. Chem. B*, 2005, **109**, 692.

45 X.-k. Kong, Z.-y. Sun, M. Chen, C.-l. Chen and Q.-w. Chen, *Energy Environ. Sci.*, 2013, **6**, 3260.

46 T. R. Mandlimath and B. Gopal, *J. Mol. Catal. A: Chem.*, 2011, **350**, 9–15.

47 C. Huang, W. Ye, Q. Liu and X. Qiu, *ACS Appl. Mater. Interfaces*, 2014, **6**, 14469–14476.

48 T. Kimura, Y. Sekio, H. Nakamura, T. Siegrist and A. P. Ramirez, *Nat. Mater.*, 2008, **7**, 291–294.

49 W. B. Wu, D. J. Huang, J. Okamoto, S. W. Huang, Y. Sekio, T. Kimura and C. T. Chen, *Phys. Rev. B*, 2010, **81**, 172409.

50 P. Zhou, H. B. Lv, M. Yin, L. Tang, Y. L. Song, T. A. Tang, Y. Y. Lin, A. Bao, A. Wu, S. Cai, H. Wu, C. Liang and M. H. Chi, *J. Vac. Sci. Technol., B*, 2008, **26**, 1030.

51 P. Tirupathi and A. Chandra, *Phys. Status Solidi B*, 2012, **249**, 1639–1645.

52 G. N. Rao, Y. D. Yao and J. W. Chen, *IEEE Trans. Magn.*, 2005, **41**, 3409–3411.

53 D. Gao, J. Qi, H. Shi, J. Zhang, Z. Zhang, D. Xue, J. Zhu and W. Sui, *Nanoscale Res. Lett.*, 2010, **5**, 769–772.

54 D. Q. Gao, G. J. Yang, J. Y. Li, J. Zhang, J. L. Zhang and D. S. Xue, *J. Phys. Chem. C*, 2010, **114**, 18347–18351.

55 A. Punnoose, H. Magnone, M. S. Seehra and J. Bonevich, *Phys. Rev. B*, 2001, **64**, 174420.

56 E. C. Stoner and E. P. Wohlfarth, *Philos. Trans. R. Soc. London*, 1948, **240**, 599.

57 H. Cölfen and M. Antonietti, *Mesocrystals and Nonclassical Crystallization*, Wiley, West Sussex, 2008.

58 H. Colfen and M. Antonietti, *Angew. Chem., Int. Ed.*, 2005, **44**, 5576.

59 N. N. Loshkareva, E. V. Mostovshchikova, A. V. Korolyov, S. V. Naumov, B. A. Gizhevskii, N. I. Solin, L. I. Naumova, S. V. Telegin and L. V. Elokhina, *J. Magn. Magn. Mater.*, 2013, **341**, 149.

60 B. X. Yang, T. R. Thurston, J. M. Tranquada and G. Shirane, *Phys. Rev. B*, 1989, **39**, 4343–4349.

61 P. J. Brown, T. Chattopadhyay, J. B. Forsyth and V. Nunez, *J. Phys.: Condens. Matter*, 1991, **3**, 4281–4287.

62 X. G. Zheng, C. N. Xu, K. Nishikubo, K. Nishiyama, W. Higemoto, W. J. Moon, E. Tanaka and E. S. Otabe, *Phys. Rev. B*, 2005, **72**, 014464.

63 L. Neel, *Low Temperature Physics*, Gordon and Breach, New York, 1962.